Optically detected magnetic resonance of photoexcited electrons in (In,Al)As/AlAs quantum dots with indirect band gap and type-I band alignment

V. Yu. Ivanov,[1] T. S. Shamirzaev,[2,4] D. R. Yakovlev,[3,5] A. K. Gutakovskii,[2] Ł. Owczarczyk,[1] and M. Bayer[3,5]

[1]*Institute of Physics, Polish Academy of Sciences, PL-02-668 Warsaw, Poland*

[2]*Rzhanov Institute of Semiconductor Physics, Siberian Branch of the Russian Academy of Sciences, 630090 Novosibirsk, Russia*

[3]*Experimentelle Physik 2, Technische Universität Dortmund, 44221 Dortmund, Germany*

[4]*Ural Federal University, 620002 Yekaterinburg, Russia*

[5]*Ioffe Institute, Russian Academy of Sciences, 194021 St. Petersburg, Russia*

(Received 3 May 2018; published 13 June 2018)

Optically detected magnetic resonance (ODMR) is measured for photoexcited electrons in (In,Al)As/AlAs quantum dots having an indirect band gap and a type-I band alignment. A sharp ODMR resonance corresponding to a g factor of 1.97 ± 0.02 is identified, associated with X-valley electrons. Its variation with optical transition energy allows us to distinguish between the spectral regions of direct and indirect QDs, which is in good agreement with the results on exciton recombination dynamics.

DOI: 10.1103/PhysRevB.97.245306

I. INTRODUCTION

The electron paramagnetic resonance (EPR) technique has been used successfully to study the spin levels and spin dynamics of point centers (impurities and defects) as well as free and localized carriers in bulk semiconductors. For low-dimensional semiconductor structures, such as quantum wells, superlattices, quantum dots (QDs), and nanocrystals, the sensitivity of the EPR technique typically is insufficient due to the small active volume [1]. This difficulty can be overcome by employing optically detected magnetic resonance (ODMR). The high sensitivity of the ODMR technique arises from measuring weakly allowed magnetic-dipole transitions not directly via microwave absorption or reflection, but indirectly through the microwave-induced changes in intensity, spectral energy, or polarization of allowed optical transitions in photoluminescence [2–4], which can be done with much higher sensitivity. Another important advantage of ODMR is its spectral selectivity, which allows one to directly link a spin resonance with a particular emission process, e.g., exciton or impurity-related recombination. Thereby, processes in different sections of a heterostructure, e.g., in a quantum well or its barriers, can be distinguished.

To date the ODMR technique has been successfully applied to a large number of low-dimensional semiconductors structures [1]. A limitation of the ODMR technique is that the optical recombination rate should be comparable to or less than the microwave-induced transition rate between the exchange and/or magnetic-field-split spin sublevels. The exciton recombination in direct-band-gap semiconductors lasting at most up to a few nanoseconds occurs typically too fast to be suitable for ODMR detection. The exciton lifetime can be extended to microseconds in AlAs/GaAs heterostructures with a type-II band alignment [5], for which ODMR has indeed been reported [3]. An alternative approach is to study nanostructures with resident carriers, e.g., CdTe/(Cd,Mg)Te quantum wells with a two-dimensional electron gas of low density, where an increase of the spin temperature of the resident electrons affects the spin-dependent formation of negatively charged trions [6]. As a result, a strong redistribution of the photoluminescence intensity between the neutral and charged excitons was observed in magnetic resonance.

The ODMR technique has been also tested for different quantum dot structures. In CdS nanocrystals embedded in phosphate glass it allows one to identify the origin of emission bands [7]. In chemically deposited CdSe nanoparticles electron and hole surface states have been studied [8]. In colloidal CdSe/CdS and CdS/HgS/CdS core-shell QDs ODMR studies of the interface properties have been performed [9]. Defect emission bands have been characterized in InP colloidal QDs [10]. Broad magnetic resonances related to holes have been reported in InAs/GaAs epitaxially grown QDs [11–13].

Recently, we demonstrated that the momentum separation of electrons and holes in heterostructures with an indirect band gap and a type-I band alignment, such as (In,Al)As/AlAs QDs, results in an increase of the exciton lifetime up to hundreds of microseconds [14]. This time appears to be sufficiently long for strong enough interaction of photogenerated carriers with microwave radiation and, therefore, these structures are promising candidates for ODMR studies, especially because long spin relaxation times were reported for electrons and excitons in (In,Al)As/AlAs structures, where the electrons reside in the X valley [15]. Another interesting property of these structures is that with the quantum confined energy variation by changing the QD size the ground electron state can be either the X or the Γ valley, i.e., the QD exciton can be either indirect or direct in momentum space [16]. Also, mixed $X - \Gamma$ exciton states were reported [17].

Here, we investigate the effect of microwave radiation with 60-GHz frequency on the magneto-optical properties of (In,Al)As/AlAs quantum dots having an indirect band gap and a type-I band alignment. We clearly identify the optically detected magnetic resonance associated with long-living photoexcited electrons in the X valley.

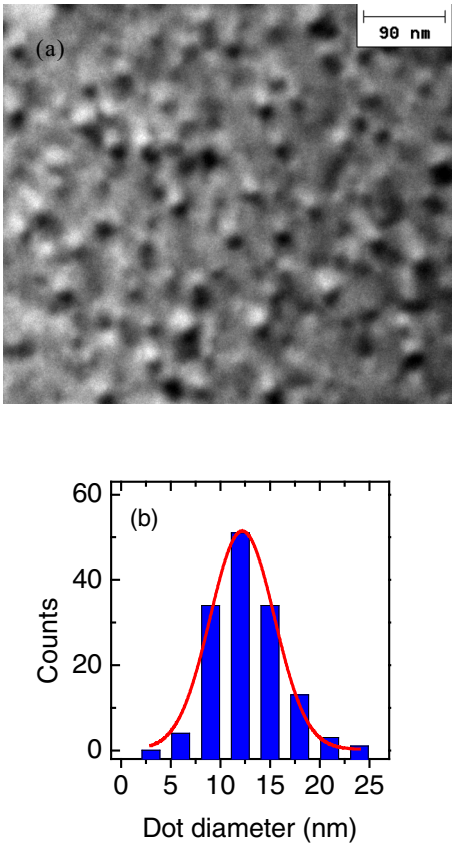

FIG. 1. TEM plane-view image (a) and the corresponding histogram of the QD-diameter distribution (b) for the studied (In,Al)As/AlAs QD heterostructure. The size dispersion fitted by a Gaussian distribution is shown by the red line.

II. EXPERIMENTAL DETAILS

The studied self-assembled (In,Al)As QDs, embedded in an AlAs matrix (structure identification number AG3686), were grown by molecular-beam epitaxy (Riber-32P system) on a semi-insulating (001)-oriented GaAs substrate. The structure contains three layers of (In,Al)As QDs sandwiched between 40-nm-thick AlAs barriers, grown on top of a 250-nm-thick GaAs buffer layer. The top AlAs barrier was protected against oxidation with a 20-nm-thick GaAs cap layer. The QDs were formed at a temperature $T_s = 515\,^{\circ}\mathrm{C}$. The nominal amount of deposited InAs in one QD layer corresponds to about 2.5 monolayers. After growth, the structure was annealed during 15 min at a temperature $T_{\mathrm{an}} = 710\,^{\circ}\mathrm{C}$, and the In and Al interdiffusion forms the QD size and composition. Technical details can be found in Ref. [14].

The QD size and density are studied by transmission electron microscopy (TEM) using a JEM-4000EX system operated at an acceleration voltage of 250 keV. A TEM plane-view image and the corresponding histogram of the QD-diameter distribution are shown in Fig. 1. The density of lens-shaped QDs in each layer is about 5.2×10^{10} cm^{-2}. The average dot diameter is $D_{\mathrm{av}} = 13.1$ nm, while the larger and smaller diameters corresponding to the upper and lower half-width of the distribution are $D_L = 15.8$ nm and smaller $D_S = 8.2$ nm. The QD size dispersion is $S_D = 100 \times (D_L - D_S)/D_{\mathrm{av}} = 57\%$. Since the shape of the photoluminescence (PL) band reflects the distribution of QD size and composition, the average composition can be evaluated from a comparison of the PL band energy with results of model calculations [18]. For the studied structures the QD composition can be determined to be $In_{0.5}Al_{0.5}As$.

The dispersion in dot size, shape, and composition within the ensemble leads to formation of (In,Al)As/AlAs QDs with different band structures, as shown in Fig. 2(a). The electron ground state changes from the Γ to the X valley with decreasing dot diameter, while the heavy-hole (hh) ground state remains at the Γ point. This corresponds to a change from a direct to an indirect band gap in momentum space, while the type-I band alignment is preserved, that is, in both cases, electron and hole are spatially confined within the (In,Al)As QDs.

Time-resolved photoluminescence is excited by the third harmonic of a Q-switched Nd:YVO_4 pulsed laser, emitted at a photon energy of 3.49 eV during a pulse duration of 5 ns. The excitation density is kept below 100 nJ/cm^2, and the pulse repetition frequency is varied from 500 Hz up to 2 kHz [14]. The photoluminescence is dispersed by a 0.5-m monochromator and detected with a CCD camera for time-integrated spectra. For time-resolved measurements a GaAs photomultiplier combined with a time-correlated photon-counting module was used. In order to monitor the PL decay across a wide temporal range up to 0.2 ms, the time resolution of the detection system is varied between 1.6 and 512 ns.

For the ODMR experiments we use an all-solid-state ultrastable microwave (MW) source operated in the range 59.25–60.75 GHz with a maximum power of 150 mW. The output MW power, P_{MW}, can be reduced by a variable attenuator down to 0.02 mW. The sample with dimensions $0.3 \times 0.6 \times 4$ mm^3 is mounted in a cylindrical microwave cavity with the main mode TE_{011} along its axes, and is placed in the maximum of the H component of the electromagnetic field. Optical excitation of the sample and detection of its photoluminescence is done via four orthogonal apertures in the cavity walls. The cavity quality (Q factor) is varied in the range 500–2500 in a regime of above-critical coupling. The cavity with the sample is placed in a split-coil magnet cryostat and exposed to a longitudinal magnetic field (Faraday geometry) up to $B = 7$ T. For low-temperature measurements it is immersed in pumped liquid helium ($T = 1.9$ K). Photoluminescence is excited by a semiconductor laser with a wavelength of 404 nm (photon energy of 3.07 eV). The excitation power (P) is varied from 1 to 25 mW. The laser excitation spot on the sample has diameter of 0.5 mm. The PL spectra in magnetic field are measured in different circular polarizations and the degree of circular polarization (DCP), defined as $P_c = (I^+ - I^-)/(I^+ + I^-)$, is analyzed. Here I^+ and I^- are the intensities of the σ^+- and σ^--polarized PL components, respectively. To determine the sign of P_c, we performed a control measurement on a diluted magnetic semiconductor structure with (Zn,Mn)Se/(Zn,Be)Se quantum wells for which $P_c > 0$ in Faraday geometry [19]. The MW power is modulated synchronously with CCD readout sequences by a p-i-n diode modulator with a dumping level of 36 dB. The PL is dispersed by a 0.5-m monochromator and synchronously detected with a CCD by switching the MW power "on" and "off." A scheme of the setup is given in Ref. [20]. The magnetic field dependences of the MW-induced signals, i.e., the ODMR signals, are recorded by scanning the magnetic field.

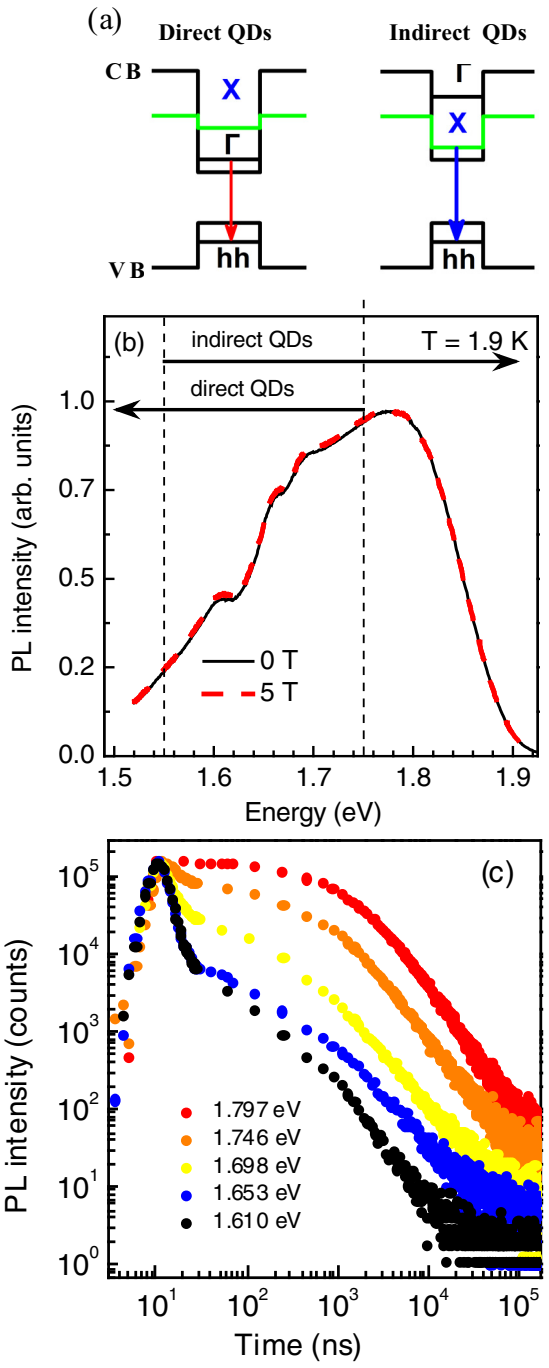

FIG. 2. (a) Band diagrams of (In,Al)As/AlAs QDs with different band structures. (b) Photoluminescence spectra of (In,Al)As/AlAs QDs measured at $B = 0$ and 5 T without polarization selectivity. (c) Time-resolved PL dynamics measured at different energies. Excitation density is $P = 40\,\mathrm{nJ/cm^2}$ and pulse repetition frequency is 1.5 kHz. The laser pulse ends at 10 ns. Note the double-logarithmic scale. Signals are normalized to their values at 10 ns delay.

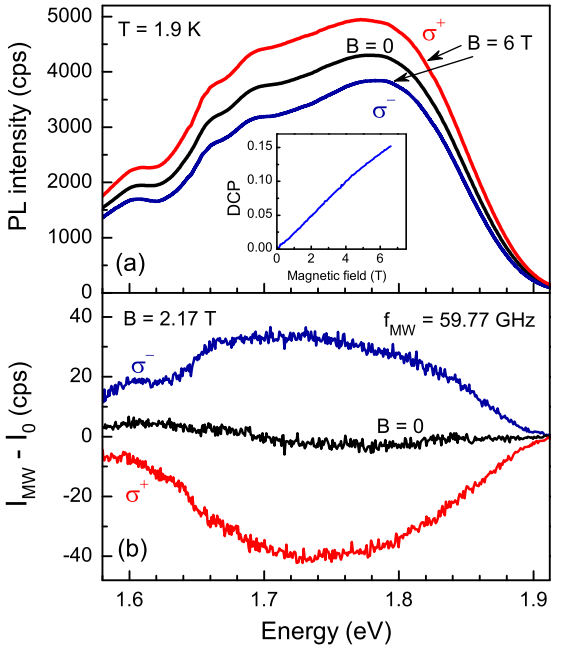

FIG. 3. (a) Photoluminescence spectra of (In,Al)As/AlAs QDs measured at $B = 0$ T (unpolarized, black line) and at $B = 6$ T (σ^+ polarized, the red line and σ^- polarized, the blue line). Inset shows the magnetic field dependence of the spectrally integrated DCP. (b) Spectral dependence of the PL intensity variation induced by the MW at $B = 0$ T and for the two circular polarizations at $B = 2.17$ T.

III. EXPERIMENTAL RESULTS

A. PL and recombination dynamics

Low-temperature PL spectra of the studied QDs are shown in Fig. 2(b). It is common for (In,Al)As/AlAs QDs that the emission band is very broad because it is contributed by recombination of direct- and indirect-band-gap QDs coexisting in the QD ensemble [16,17]. The contributions of the two types of QDs can be distinguished by their very different recombination dynamics, which is short in the direct-band-gap QDs and long in the indirect-band-gap QDs.

The PL dynamics measured at various energies are shown in Fig. 2(c). The data are plotted on a double-logarithmic scale, which is convenient for presenting the dynamics across a wide range of decay times and PL intensities. At high energies (>1.75 eV) the exciton recombination has two distinctive stages: (i) a relatively flat decay immediately after the excitation pulse lasting up to approximately 1 μs and, subsequently, (ii) a stronger decay, which can be described by a power-law function. Such a dynamics results from superposition of multiple monoexponential decays with different times varying with size, shape, and composition of the indirect-band-gap QDs [14]. At low energies (1.55–1.75 eV) an additional fast decay provided by direct-band-gap QDs appears. The fraction of these QDs increases with decreasing PL energy transition, i.e., with increasing QD size. With increasing dot diameter, the Γ valley shifts to lower energies more strongly than the X valley due to the smaller effective mass of the Γ-valley electrons. For a particular dot diameter, the Γ and X electron levels intersect. The $\Gamma - X$ crossing energy is spread over the energy range of 1.55–1.75 eV due to the variation of the QD parameters [16,17] [see Fig. 2(b)].

The application of external magnetic fields does not affect the PL intensity and spectrum shape [see Fig. 2(b)], but the emission has become circularly polarized. One can see in Fig. 3(a) that at $B = 6$ T the σ^+-polarized PL component

is more intense than the σ^--polarized one, so that P_c is positive. In order to avoid carrier optical orientation, we use in this experiment linearly polarized laser light that excites photocarriers nonresonantly with large excess energy. Under these conditions the degree of circular polarization of the PL reflects the thermal population of the exciton Zeeman sublevels split by the magnetic field [21]. The long recombination times of the indirect excitons provide an equilibrium population of the Zeeman sublevels. The magnetic field dependence of the DCP, shown in the inset of Fig. 3(a), scales linearly with magnetic field up to 7 T. Note that the positive DCP in the studied nominally undoped QDs allows us to exclude a possible contribution of negatively charged excitons (trions) to the QD emission, as for trions a negative DCP is expected [15].

B. Optically detected magnetic resonance

When ODMR is performed, several contributions to the MW-induced changes of the photoluminescence can be considered [22]. They are: (i) a spectral shift of the PL line, which is not relevant for the indirect QDs with their very broad emission band; (ii) a variation of the PL intensity, i.e., a redistribution between the radiative recombination channels or between radiative and nonradiative recombination; and (iii) changes in the DCP. In Fig. 3(b) the MW-induced changes, $I_{\mathrm{MW}} - I_0$, of the intensities of unpolarized and polarized PL are shown for $B = 2.17$ T. Here I_{MW} and I_0 are the PL intensities with and without MW application, respectively. One sees that for the unpolarized PL variation of the intensity is very small. Therefore, we conclude that the second contribution (ii) is negligible for the studied structures. On the other hand, pronounced changes are seen for the circularly polarized PL corresponding to a signal decrease for the σ^+-polarized PL component and a signal increase for the σ^--polarized one. This means that the DCP decreases under MW application, i.e., the contribution (iii) is dominant for our case.

For analyzing the ODMR signal, it is convenient to consider the variation of the normalized PL intensity: $(I_{\mathrm{MW}} - I_0)/I_0$. The magnetic field dependence of this ODMR signal measured for the σ^+-polarized PL component is given in Fig. 4(a). Here, the PL signal was integrated across the whole PL band in the spectral range from 1.55 to 1.90 eV. Similar signals are observed for positive and negative magnetic fields, just with a sign reversal caused by the measurement for a fixed circular polarization. The linear dependencies of the ODMR signal on laser power and MW power shown in Figs. 4(b) and 4(c) confirm that for the chosen experimental conditions the response of QDs is in the linear regime.

The magnetic field dependence of the ODMR signal in Fig. 4(a) has two contributions. One is a very broad signal that starts from weak magnetic fields and extends up to 5 T. It can be related to nonresonant heating of the carrier spin system, in which both photogenerated electrons and hole are involved. Such appearances have been reported for ODMR signals in CdTe/(Cd,Mg)Te quantum wells with a two-dimensional electron gas of low density [6] and in diluted magnetic semiconductor quantum wells (Zn,Mn)Se/(Zn,Be)Se [22].

Another contribution to the ODMR signal is the narrow resonance at $B_R = 2.17$ T, which is shown in more detail in Fig. 5. It can be well fitted by a Lorentz function with

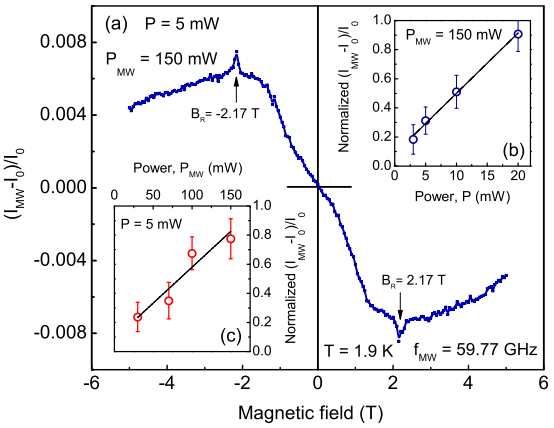

FIG. 4. (a) Magnetic field dependence of the ODMR signal for the σ^+-polarized PL component, integrated across the whole PL spectrum (1.55–1.90 eV). (b) ODMR signal as a function of laser power measured for a MW power of 150 mW. (c) ODMR signal as a function of MW power measured for a laser power of 5 mW. Lines in panels (b,c) are linear interpolations. Data in panels (b,c) are measured at $B_R = 2.17$ T.

the maximum position at $B_R = 2.17 \pm 0.02$ T (corresponding to a g factor of 1.97 ± 0.02) and a width of $\Delta B_R = 17 \pm 0.5$ mT. Its slight asymmetry is related to contribution of the nonresonant background.

Recently, we demonstrated by spin-flip Raman scattering that in indirect band gap (In,Al)As/AlAs QDs the g factor of an X-valley electron is isotropic and has a value of about $+2$,

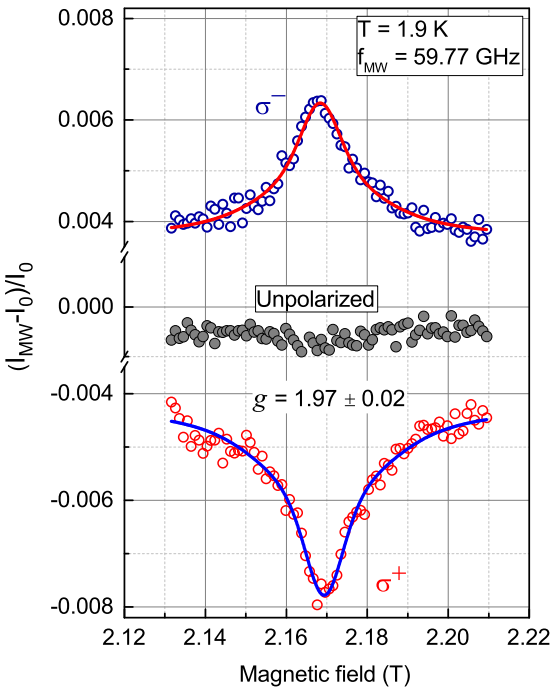

FIG. 5. Magnetic field dependence of the ODMR signal for the PL integrated across the whole PL spectrum (1.55–1.90 eV) in the vicinity of the resonance field $B_R = 2.17$ T. $P_{\mathrm{MW}} = 150$ mW. Strong changes are detected only for the circularly polarized PL. Lines are fits with Lorentz functions.

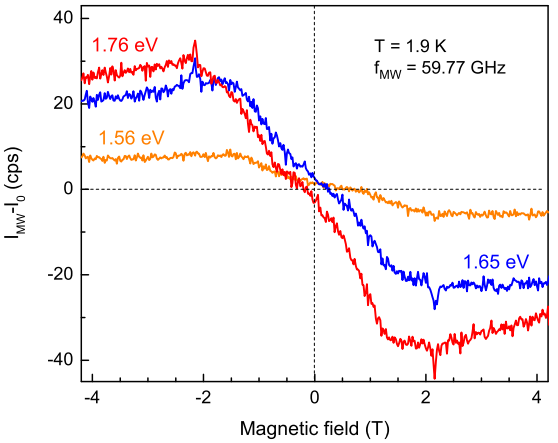

FIG. 6. Magnetic field dependence of the PL intensity variation induced by the MW for the σ^+-polarized PL component measured at energies of 1.56, 1.65, and 1.76 eV. $P_{MW} = 150$ mW.

while the heavy-hole longitudinal g factor is also positive and exceeds the electron g factor [17]. This allows us to assign the observed ODMR resonance to resonant MW heating of the photoexcited X-valley electrons. The g factor of these electrons has a very small dispersion, which is in line with the narrow linewidth of the resonance. The detection of ODMR signal on photogenerated carriers becomes possible due to their long recombination time caused by the indirect band gap [see Fig. 2(c)].

The ODMR signal has the spectral dependence shown in Fig. 6, where the PL intensity variation induced by the MW is plotted as a function of magnetic field for the three energies of 1.56, 1.65, and 1.76 eV. The smaller signal intensity at 1.56 eV is mainly related to the smaller PL intensity there, because the presented data are not normalized on the PL intensity. The broad nonresonant signal does not show a strong dependence on the spectral position, but the narrow resonance is detectable only at 1.65 and 1.76 eV. We plot the spectral dependence of the ODMR signal of the narrow resonance in Fig. 7(b). Obviously it is present only in the spectral range where the contribution of the indirect QDs has been confirmed by the recombination dynamics, see also Fig. 2. The PL spectrum marked with the regions for direct and indirect QDs is given for comparison in Fig. 7(a).

IV. CONCLUSIONS

Pronounced effects of MW heating of photogenerated electrons have been found in (In,Al)As/AlAs QDs having an indirect band gap and a type-I band alignment. A sharp ODMR resonance corresponding to a g factor of 1.97 ± 0.02 is identified, arising from the photoexcited electrons in the X valley. Its spectral dependence allows us to identify the spectral ranges of direct and indirect QDs, which are in good agreement with results on the exciton recombination dynamics. An ODMR resonance related to long-living photoexcited holes has not been resolved yet, most probably due to the large dispersion of the hole g factor, which causes a broadening of the ODMR resonance.

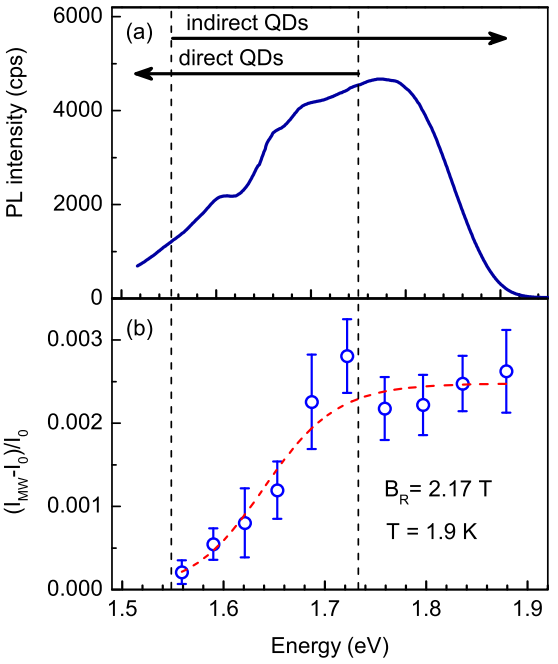

FIG. 7. (a) Photoluminescence spectrum of the (In,Al)As/AlAs QDs measured at $B_R = 2.17$ T. Ranges with indirect and direct QDs are marked by the dashed lines and arrows. (b) Spectral dependence of the resonant ODMR signal. Red line is guide for the eye.

ACKNOWLEDGMENTS

This work was supported by the Deutsche Forschungsgemeinschaft via ICRC TRR160 (Project B4) and the Russian Foundation for Basic Research (Grant No. 16-02-00242), as well as by the Act 211 Government of the Russian Federation (Contract No. 02.A03.21.0006). T.S.S. acknowledges support from the Federal Agency for Scientific Organizations (Grant No. AAAA-A17-117042110141-5). V.Yu.I. acknowledges support from the Polish National Science Center (Grant No. DEC-2014/14/M/ST3/00484).

[1] P. G. Baranov, H. J. von Bardeleben, F. Jelezko, and J. Wrachtrup, *Magnetic Resonance of Semiconductors and Their Nanostructures: Basic and Advanced Applications* (Springer, Wien, Austria, 2017).

[2] B. C. Cavenett, Optically detected magnetic resonance (O. D. M. R.) investigations of recombination processes in semiconductors, Adv. Phys. **30**, 475 (1981).

[3] P. G. Baranov and N. G. Romanov, Magnetic resonance in micro- and nanostructures, Appl. Magn. Reson. **21**, 165 (2001).

[4] M. Godlewski, W. M. Chen, and B. Monemar, Optical-detection of cyclotron resonance for characterization of recombination processes in semiconductors, CRC Crit. Rev. Solid State Mater. Sci. **19**, 241 (1994).

[5] T. S. Shamirzaev, J. Debus, D. R. Yakovlev, M. M. Glazov, E. L. Ivchenko, and M. Bayer, Dynamics of exciton recombination in strong magnetic fields in ultrathin GaAs/AlAs quantum wells with indirect band gap and type-II band alignment, Phys. Rev. B **94**, 045411 (2016).

[6] C. Y. Hu, W. Ossau, D. R. Yakovlev, G. Landwehr, T. Wojtowicz, G. Karczewski, and J. Kossut, Optically detected magnetic resonance of excess electrons in type-I quantum wells with a low-density electron gas, Phys. Rev. B **58**, R1766 (1998).

[7] E. Lifshitz, I. D. Litvin, H. Porteanu, and A. A. Lipovskii, Magneto-optical properties of CdS nanoparticles embedded in phosphate glass, Chem. Phys. Lett. **295**, 249 (1998).

[8] E. Lifshitz, I. Dag, I. D. Litvitn, and G. Hodes, Optically detected magnetic resonance study of electron/hole traps on CdSe quantum dot surfaces, J. Phys. Chem. B **102**, 9245 (1998).

[9] E. Lifshitz, A. Glozman, I. D. Litvin, and H. Porteanu, Optically detected magnetic resonance studies of the surface/interface properties of II-VI semiconductor quantum dots, J. Phys. Chem. B **104**, 10449 (2000).

[10] L. Langof, E. Ehrenfreund, E. Lifshitz, O. I. Micic, and A. J. Nozik, Continuous-wave and time-resolved optically detected magnetic resonance studies of nonetched/etched InP nanocrystals, J. Phys. Chem. B **106**, 1606 (2002).

[11] N. Zurauskiene, G. Janssen, E. Goovaerts, A. Bouwen, D. Schoemaker, P. M. Koenraad, and J. H. Wolter, Optically detected microwave resonance at 95 GHz of exciton states in InAs/GaAs quantum dots, Phys. Status Solidi B **224**, 551 (2001).

[12] G. Janssen, E. Goovaerts, A. Bouwen, B. Partoens, B. Van Daele, N. Zurauskiene, P. M. Koenraad, and J. H. Wolter, Observation of cyclotron resonance in an InAs/GaAs wetting layer with shallowly formed quantum dots, Phys. Rev. B **68**, 045329 (2003).

[13] N. Žurauskienė, G. Janssen, E. Goovaerts, M. Godlewski, V. Yu. Ivanov, and P. M. Koenraad, A 60 GHz microwave resonance investigation of shallowly formed InAs quantum dots embedded in GaAs, Proc. SPIE **6596**, 659609 (2007).

[14] T. S. Shamirzaev, J. Debus, D. S. Abramkin, D. Dunker, D. R. Yakovlev, D. V. Dmitriev, A. K. Gutakovskii, L. S. Braginsky, K. S. Zhuravlev, and M. Bayer, Exciton recombination dynamics in an ensemble of (In, Al)As/AlAs quantum dots with indirect band-gap and type-I band alignment, Phys. Rev. B **84**, 155318 (2011).

[15] D. Dunker, T. S. Shamirzaev, J. Debus, D. R. Yakovlev, K. S. Zhuravlev, and M. Bayer, Spin relaxation of negatively charged excitons in (In, Al)As/AlAs quantum dots with indirect band gap and type-I band alignment, Appl. Phys. Lett. **101**, 142108 (2012).

[16] T. S. Shamirzaev, A. V. Nenashev, and K. S. Zhuravlev, Coexistence of direct and indirect band structures in arrays of InAs/AlAs quantum dots, Appl. Phys. Lett. **92**, 213101 (2008).

[17] J. Debus, T. S. Shamirzaev, D. Dunker, V. F. Sapega, E. L. Ivchenko, D. R. Yakovlev, A. I. Toropov, and M. Bayer, Spin-flip Raman scattering of the Γ-X mixed exciton in indirect band gap (In, Al)As/AlAs quantum dots, Phys. Rev. B **90**, 125431 (2014).

[18] T. S. Shamirzaev, A. V. Nenashev, A. K. Gutakovskii, A. K. Kalagin, K. S. Zhuravlev, M. Larsson, and P. O. Holtz, Atomic and energy structure of InAs/AlAs quantum dots, Phys. Rev. B **78**, 085323 (2008).

[19] D. Keller, D. R. Yakovlev, B. König, W. Ossau, Th. Gruber, A. Waag, L. W. Molenkamp, and A. V. Scherbakov, Heating of the magnetic ion system in (Zn, Mn)Se/(Zn, Be)Se semimagnetic quantum wells by means of photoexcitation, Phys. Rev. B **65**, 035313 (2001).

[20] V. Yu. Ivanov, M. Godlewski, D. R. Yakovlev, S. M. Ryabchenko, G. Karczewski, and A. Waag, Time-resolved optically-detected magnetic resonance of II-VI diluted-magnetic-semiconductor heterostructures, Phys. Status Solidi A **204**, 174 (2007).

[21] T. S. Shamirzaev, J. Rautert, D. R. Yakovlev, J. Debus, A. Yu. Gornov, M. M. Glazov, E. L. Ivchenko, and M. Bayer, Spin dynamics and magnetic field induced polarization of excitons in ultrathin GaAs/AlAs quantum wells with indirect band gap and type-II band alignment, Phys. Rev. B **96**, 035302 (2017).

[22] V. Yu. Ivanov, M. Godlewski, D. R. Yakovlev, M. K. Kneip, M. Bayer, S. M. Ryabchenko, and A. Waag, Optically detected magnetic resonance in (Zn, Mn)Se/(Zn, Be)Se quantum wells, Phys. Rev. B **78**, 085322 (2008).